COBEM 2023 27TH INTERNATIONAL CONGRESS OF MECHANICAL ENGINEERING

ABCM Brazilian Society of Mechanical Sciences and Engineering
27th ABCM International Congress of Mechanical Engineering
December 04-08, 2023, Florianópolis-SC, Brazil

COBEM-2023-1850

DEVELOPMENT OF A NUMERICAL HEAT TRANSFER MODEL VIA FEM FOR TRANSPORT AND STORAGE OF BIOLOGICAL MATERIAL AND VACCINES BASED ON PELTIER EFFECT

Felipe Neto
Arthur Claydson
Federal Institute of Pernambuco – Recife Campus - Av. Prof. Luiz Freire, 500, Cidade Universitária, Recife – PE.
fran@discente.ifpe.edu.br
acrgl@discente.ifpe.edu.br

Andrezza Tomás
Federal Institute of Pernambuco – Recife Campus - Av. Prof. Luiz Freire, 500, Cidade Universitária, Recife – PE.
andrezzaoliveira@recife.ifpe.edu.br

José Ângelo Peixoto da Costa
Federal Institute of Pernambuco – Recife Campus - Av. Prof. Luiz Freire, 500, Cidade Universitária, Recife – PE.
angelocosta@recife.ifpe.edu.br

Alvaro Ochoa
Federal Institute of Pernambuco – Recife Campus - Av. Prof. Luiz Freire, 500, Cidade Universitária, Recife – PE.
ochoaalvaro@recife.ifpe.edu.br

Abstract. *Development of a numerical heat transfer model via a steady-state thermal-electric FEM solver for the transport and storage of biological materials and vaccines, among others, based on the Peltier effect. Biological materials require specific storage temperatures Currently, the most used method is through a box made of expanded polystyrene, containing reusable dry ice in the form of tubes/plates (or just ice), which can have temperature changes while transportation, damaging the materials (organs, medications, vaccines, etc.) since there is no adequate temperature control. The only existing control (which is not a real control) is the insertion of a thermocouple to verify the internal temperature of the box. Despite the advantages of using Peltier cells as an organ preservation system, numerical studies are needed to prove their effectiveness in applications, such as organ conditioning. One of the difficulties encountered is related to the heat transfer process within the box, as well as the type of material to be used because of its thermal conductivity and the type of heat exchanger that allows the dissipation of heat from the hot face of the thermoelectric cell. Nevertheless, this work aims to develop a numerical model using the FEM technique and the Ansys steady-state thermal electric tool as a computational platform as a reference base for the operating conditions for the storage box of biological material, vaccines, medications, among others; it's also expected the simulation verify if the thermoelectric cell (at first moment without any material in his cold surface and after with a aluminum plate coupled) will be able to reach the temperature of 4ºC to 9ºC according to the temperature values for transporting organs defined by the National Heat Surveillance Agency (ANVISA). The numerical results are expected to establish the initial parameters for the construction of an experimental prototype based on the Peltier effect.*

Keywords: *Heat Transfer Model, Ansys Simulation, Peltier, Biological Material Transport Box, Thermoelectric Cooler.*

1. INTRODUCTION

In present days, according to the Brazilian Association of Organ Transplantation (ABTO), Brazil has the world's largest public program for organ, tissue, and cell transplantation, providing access to a significant portion of the population through the Unified Health System (SUS) which funds 88% of the transplants in the country.

Besides determining how organ transportation will be carried out, one of the crucial factors is how it will be transported, meaning the box that will be used.

(Canuto et al., 2018) stated that the transport of biological materials, more precisely organs, occurs through a polystyrene thermal box that contains dry ice. The goal is to maintain the hypothermic state of the material because, depending on what is being transported, specific temperatures must be reached. For instance, the heart must remain at 4°C from the moment it is removed from the recipient until it reaches the donor.

The booklet of the Transplant League of the State University of Campinas (Unicamp, 2019) reports that organs are extremely sensitive, especially to temperature and ischemia time, which refers to the time that generates a lack or reduction of blood supply to the tissue. When it comes to tissues, such as vessels and tendons, what determines their validity is the way they were stored.

There are several works carried out in recent years with thermoelectric devices, both in the health field, for example, to transport refrigerated insulin in remote or hard-to-reach areas (Nohay et al, 2020), development of a portable device for vaccine transportation (Ivanov et al, 2021) as well as in the field of physics, aiming to analyze the behavior of spins in the Peltier effect, which in short, modulates the temperature of the magnetic junction in response to current spins (Daimon et al, 2016).

According to (Antonova et al, 2005) finite element methods have become extremely essential for problem-solving in various engineering fields. This is because it allows visualizing the system's behavior even before his construction, avoiding unnecessary expenses in the future due to possible technical failures or unexpected malfunctions. This method has the versatility to shape structures, work with complex materials, and apply different types of loads and boundary conditions, making it suitable for many types of equations and situations.

According to what has been explained, there is an outdated technology that persists in transportation of human biological material, animal specimens, blood components, medications, and vaccines, which are currently carried out using a thermal polystyrene cooler containing reusable dry ice in the form of tubes/plates. The results presented here refers to the computational numerical simulation of heat transfer by finite elements through Ansys software, of a thermoelectric device using steady-state thermal-electric conditions. The methodology adopted for the simulation is described, initially focusing on a p-type and n-type junction and subsequently on a complete thermoelectric device model TEC-12706. Finally, the comparison of results with a real experiment conducted in a laboratory will be presented.

2. **METHODOLOGY**

This topic will be introduced in the following chronological order. Initially, the Finite Element Method (FEM) simulation of an n-type and p-type junction is presented, followed by a complete composition of a thermoelectric device, and finally, the comparison of the results with a real experiment conducted on the bench.

Mathematical models of TECs (thermoelectric coolers) already exist in the literature and are discussed by several authors such as (Bhuiyan et al, 2019), (Seifert et al, 2002), (Antonova et al, 2005), (Jangle et al, 2008), and (Chen et al, 2020). However, mathematical modeling is not the objective of this work. Nevertheless, the equations governing thermo-electric systems will be presented so that they can be coupled with a finite element modeling, as proposed by (Antonova et al, 2005).

Eq.(1) relates to the heat flow, and Eq.(2) refers to the continuous electrical charge, which are coupled to a set of thermoelectric equations Eq.(3), (4).

$$\rho C \frac{\partial T}{\partial t} + \nabla . q = \dot{q} \tag{1}$$

$$\nabla . \left(J + \frac{\partial D}{\partial t} \right) = 0 \tag{2}$$

$$q = [\Pi] . J - [\lambda] . \nabla T, \tag{3}$$

$$J = [\sigma] . (E - [\alpha] . \nabla T) \tag{4}$$

where ρ is the density in kg/m³, C is the specific heat in J/(Kg-K), T is the temperature in K (Kelvin), $\dot{q}$ is the heat generation per unit volume in W/m³, q is the heat flux vector in W/m², J is the electric current density vector in A/m², E is the intensity vector of the electric field in V/m, D is the electric flux density vector in C/m², [λ] is the thermal conductivity matrix in W/m-K, [σ] is the electrical conductivity matrix in S/m, [α] is the Seebeck coefficient matrix in V/K, and [Π]=T[α] is the matrix of the Peltier effect in V.

And the Eq.(5) for the average dielectric is given by:

$$D = [\varepsilon] . E \tag{5}$$

where [ε] is the matrix of dielectric permittivity in F/m.

When we do not have a magnetic field varying with time, the electric field E is irrotational ($\nabla \times E = 0$) and can now be derived from the electric scalar potential φ Eq.(6).

$$E = -\nabla . \varphi \tag{6}$$

Replacing Eqs.(3), (6) into Eqs.(1), (2) generates a coupled system of thermo-electric equations Eqs.(7), (8).

$$\rho C \frac{\partial T}{\partial t} + \nabla . ([\Pi] . J) - \nabla . ([\lambda] . \nabla T) = \dot{q} \tag{7}$$

$$\nabla . \left([\varepsilon] . \nabla . \frac{\partial \varphi}{\partial t} \right) + \nabla . ([\sigma] . [\sigma] . \nabla T) + \nabla . ([\sigma] . \nabla \varphi) = 0 \tag{8}$$

In which the heat generation $\dot{q}$ in Eq.(7) now includes the electrical power J. And during the Joule effect and the work against the Seebeck effect [α].∇T.

2.1 FEM SIMULATION OF N-TYPE AND P-TYPE JUNCTION

To start with the FEM simulation procedure, we will use the method employed by (Antonova et al, 2005) and introduced by (Silvester et al, 1996), in which the finite element equations of a thermoelectric system can be obtained by applying the Galerkin procedure to finite elements. This technique involves 4 steps. The first step is the approximation of the temperature T and the scalar electric power φ by a finite element Eq.(9), (10).

$$T = N . T_e \tag{9}$$

$$\varphi = N . \varphi_e \tag{10}$$

where N is the vector of functions with the size of the element, T_e is the nodal vector of temperatures, and φ_e is the nodal vector of electrical powers.

Then, Eq.(7) and (8) are rewritten in a weak projective form, and the integration of these weak projective equations is performed by parts. Finally, the Neumann boundary conditions (Incropera et al, 2019) are applied, resulting in a system of thermo-electric equations using finite element method, given by Eq.(11).

$$[C^{TT}\ 0\ 0\ C^{\varphi\varphi}]\{\dot{T}_e\ \dot{\varphi}_e\} + [K^{TT}\ 0\ K^{\varphi T}\ K^{\varphi\varphi}]\{T_e\ \varphi_e\} = \{Q + Q^P + Q^e\ I\} \tag{11}$$

in which the elements of the matrices and the load vectors are obtained through numerical integration using Gauss Quadrature from the volumetric element V. The elements of the matrices are given by Eq.(12), (13), (14), (15), (16), (17), (18), (19), respectively.

$$K^{TT} = \int_V \nabla N . [\lambda] . \nabla N\ dV \tag{12}$$

$$K^{\varphi\varphi} = \int_V \nabla N . [\sigma] . \nabla N\ dV \tag{13}$$

$$K^{\varphi T} = \int_V \nabla N . [\sigma][\sigma] . \nabla N\ \ dV \tag{14}$$

$$C^{TT} = \rho \int_V CNN\ dV \tag{15}$$

$$C^{\varphi\varphi} = \int_V \nabla N . [\varepsilon] . \nabla N\ dV \tag{16}$$

$$Q^P = \int_V \nabla N . [\Pi] . J\ dV \tag{17}$$

$$Q^e = \int_V NE . J\ dV \tag{18}$$

The Eq.(12) is the thermal stiffness matrix, Eq.(13) is the electric stiffness matrix, Eq.(14) the Seebeck stiffness matrix, Eq.(15) the thermal damping matrix, Eq.(16) the dielectric damping matrix, Q is the vector of combined heat generation loads, Eq.(17) peltier heat load vector and Eq.(18) the electric power load vector.

The thermal loads can be worked in the form of temperature, heat flow, heat flow per surface, convection, radiation, or even the generation of internal heat in the body caused by the dissipation of electrical power, accounted for by the term Q^e. Electrical loads can also be worked in the form of electrical power or electrical current point. Based on the description (Antonova et al, 2005) and grounded in (Silvester et al, 1996), the input parameters of the matrices, performed by the software Ansys, are [λ], [σ], [α], [ε], in the form of terms on the diagonal. This type of information input can be combined with an arbitrary orientation of elements in the coordinate system, considering the material orientation as an alternative. In short, we will introduce the electric current as the first boundary condition; as the second, we will impose that we can control the temperature of the hot side of the TEC through a heat exchanger.

As output, the analysis of how much temperature will be absorbed from the cold side of the TEC is expected. This procedure will also be repeated for simulating a complete TEC (not just a junction). From the flowchart in Figure 1, we can understand the methodology employed to analyze a junction. Table 1 contains the data used for this simulation, such

as junction dimensions, material properties (McKnight, 2010), element order, element size, defined ambient temperature, hot-side boundary conditions, and voltage and current boundary conditions.

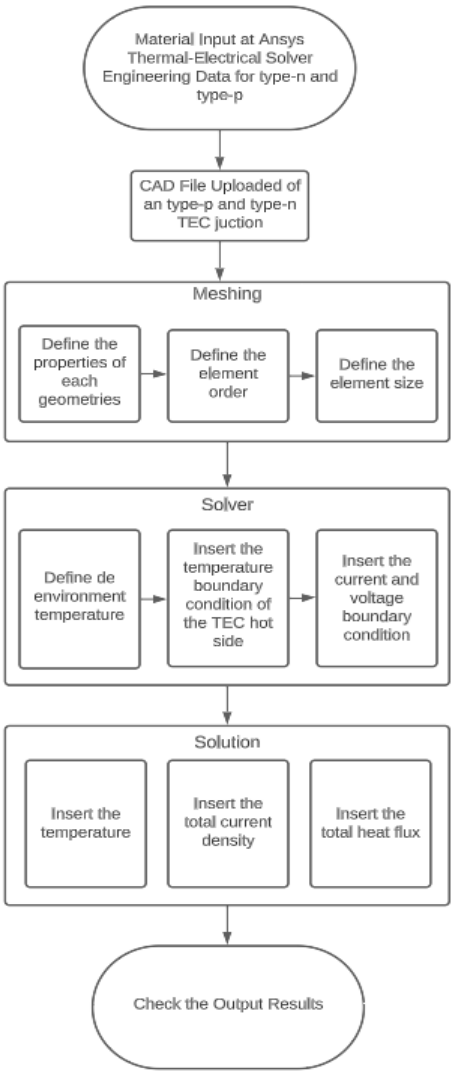

Figure 1. Simulation methodology for an N-P type junction of a TEC.

At Table 1, there are the properties of Bi2Te3 used in the simulation and by (McKnight, 2010).

Table 1. Properties of the Bi2Te3 used in type-p and type-n junction of an TEC.

Type-N and Type-P Junction Information	
Properties of Bi2Te3	
Type-P Seebeck coefficient, V/°C	240E-6
Type-N Seebeck coefficient, V/°C	-240E-6
Thermal conductivity, W/mºC	2
Resistivity, Ωm	1E-5

In Figure 2, we have the 3D view of one of the numerous N-Type and P-Type junctions.

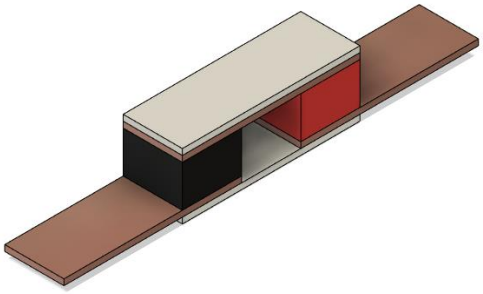

Figure 2. N-Type and P-Type 3D Junction.

In Table 2, the dimensions used are described, following (Barrubeeah et al., 2021). It is emphasized that L represents the length, W represents the width, and T represents the thickness.

Table 2. TEC Junction Dimension

Dimensions of the TEC Junction	
Details	**Values**
N-Type (Black Block), mm	1 (L) x 1 (W) x 0.70 (T)
P-Type (Red Block), mm	1 (L) x 1 (W) x 0.70 (T)
Alumina 96% (White Stripe), mm	3 (L) x 1 (W) x 0.10 (T)
Copper (Raw Copper), mm	3 (L) x 1 (W) x 0.10 (T)

In Table 3, we present the order of the element, element size, defined ambient temperature, boundary condition applied to the hot side, voltage and current boundary conditions.

Table 3. Conditions applied to the junction.

Meshing and Boundary Conditions		
Meshing	Element Order	Quadratic
	Element Size, mm	0.1
Boundary Conditions	Ambient Temperature, °C	25
	Temperature Hot Face, °C	40
	Voltage, V	0
	Current, A	2

2.2 FEM SIMULATION OF A THERMOELECTRICAL COOLER

For the simulation of a complete TEC (first bench experiment), the following boundary conditions are shown in Table 4, and for the second in Table 5. The dimensions of each N-P-type junction are the same as those listed in Table 2; the only difference is that there is a set of 128 junctions within an area of 30 × 30 mm. These junctions are in the middle, and there are two 96% alumina plates at their ends. Figure 3 shows the structure and BC's of the simulated TEC.

Table 4. Conditions Applied at a TEC.

Meshing and Boundary Conditions		
Meshing	Element Order	Quadratic
	Element Size, mm	0.5
Boundary Conditions	Ambient Temperature, °C	25
	Temperature Hot Face, °C	62
	Voltage, V	0
	Current, A	2

Table 5. Conditions Applied at the case where the TEC will be working daily.

Meshing and Boundary Conditions		
Meshing	Element Order	Quadratic
	Element Size, mm	0.5
Boundary Conditions	Ambient Temperature, °C	24
	Temperature Hot Face, °C	27
	Voltage, V	0
	Current, A	2

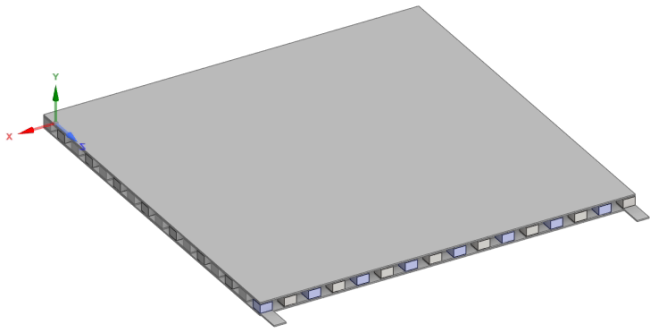

Figure 3. Full TEC with 128 couples.

2.3 BENCH EXPERIMENTALS

Considering the validation of the computational numerical simulation using the steady-state thermal-electric solver, there was the possibility of setting up a bench test in the laboratory and applying the same conditions imposed in the numerical simulation; the only difference is that, in the numerical simulation, we do not have the heat sink attached to the hot side of the TEC; thus, the situation where the temperature on the hot side is the temperature that the heat sink could remove was considered.

At Figure 4 and Figure 5, we can see how the temperature measurement procedure was carried out both for the ambient temperature, temperatures on the cold and hot faces. These measurements were taken with a DS18B20 temperature sensor, connected to an Arduino Uno microcontroller (to receive the data), and Microsoft Excel software (2023 version) to capture the data, which was being displayed on the microcontroller's serial monitor through the data stream function.

For powering the TEC, direct current source is used, and to control the operation of the TEC, relays have been added to switch based on a defined set-point.

Figure 4. Hardware assembled for the experimental simulation.

3. RESULTS

In the first case, the understanding of the behavior of a N-P type junction was sought based on current and voltage input. Regarding the voltage, it has a value of zero (as if the end of the circuit were grounded) meaning the current enters through the N leg, passes through the system, and is grounded at the end of the P leg.

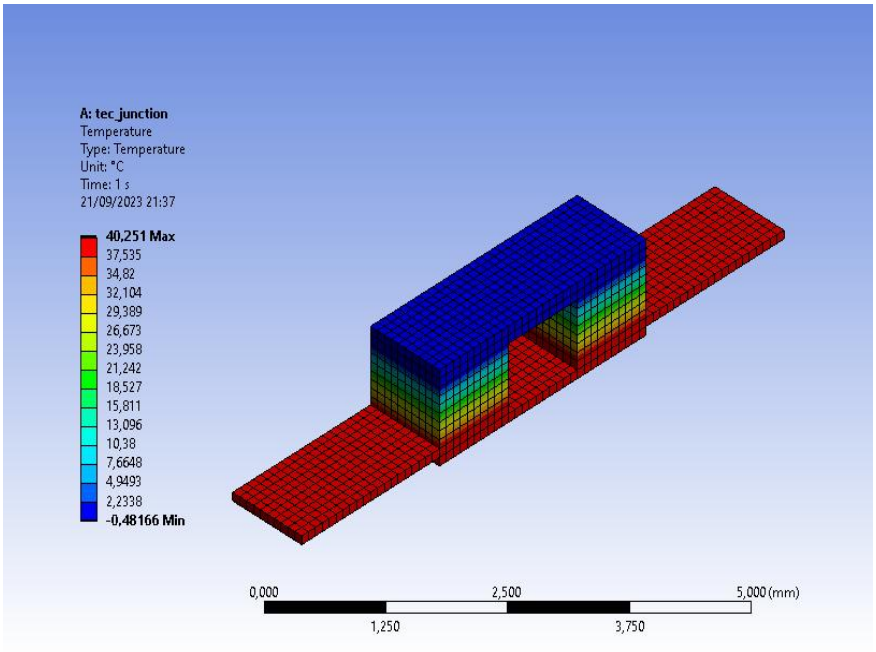

Figure 5. Temperature gradient in an N-P type TEC junction.

As shown in Figure 5, it is possible to confirm that there is a decrease in the temperature based on the imposed conditions from Table 3. On the cold side, it reached values of - 0.48°C, and on the hot side, at 40°C. Despite being only a junction of hundreds of N-P types of elements forming a TEC, this result indicates that it will be able to achieve the specified values for cooling the organs mentioned earlier. However, to confirm this hypothesis, we performed numerical and experimental simulations of a complete TEC.

As we did not have the possibility to simulate a N-P type junction in our laboratory, we proceeded to simulate a complete TEC since this is the configuration that will be used in the real prototype; with a complete TEC, were started both numerical and experimental case.

The experimental condition imposed on (which validated the numerical model) was with the fanless heat sinks and the laboratory air conditioning turned off, indicating that the system was at room temperature (approximately 25 °C) under the same conditions as those listed in Table 4, which was imposed on the numerical side. Fig. 6 shows the results obtained from the experiment.

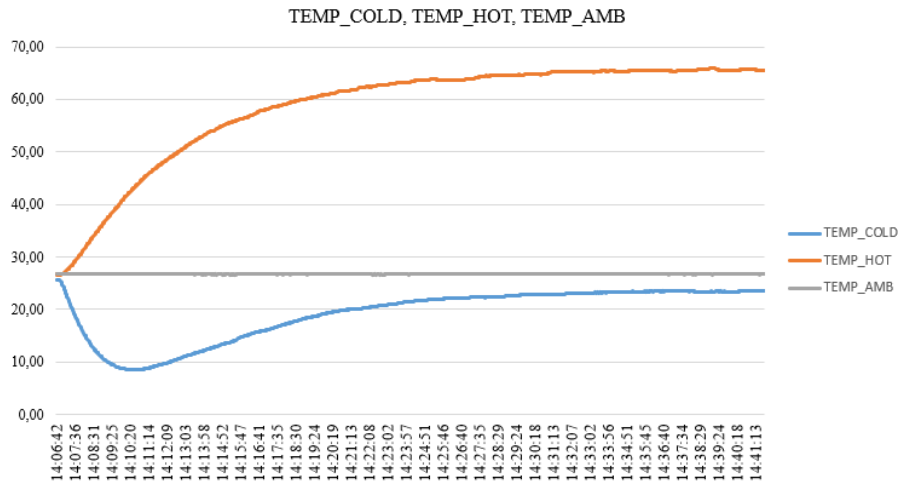

Figure 6. Temperature versus time graph of a complete TEC

Where there is TEMP_COLD, TEMP_HOT, and TEMP_AMB, they respectively represent the temperature on the cold face, temperature on the hot face and the ambient temperature (with a color distinction for each type of variable). On the X-axis is the simulation time and on the Y-axis the temperature, thus forming a graph of temperature as a function of time.

When the experiment was initiated, all values were in equilibrium, but over time, the temperature on the hot side increased and on the cold side decreased until a certain point, at which the Joule effect started to influence significantly, raising the temperature on the cold side and instead of cooling the TEC, begins to be heated. This occurred because the heat sink could not dissipate much energy by natural convection, raising an alert about the need to introduce forced convection between the fins of the heat sink to enhance the heat transfer from the hot side.

From the numerical perspective of the experiment mentioned above, it was not possible to run it under transient conditions because until now, it has not existed for the solver used in the ANSYS software.

In Figure 7, the Joule effect is repeated, and unfortunately, there is no way to verify the TEC situation at a desired moment in time, as it is a simulation in steady state rather than transient. Although, which confirms the validation of the process used to understand the working of a TEC, by applying the same conditions as the experiment, we achieved the same results.

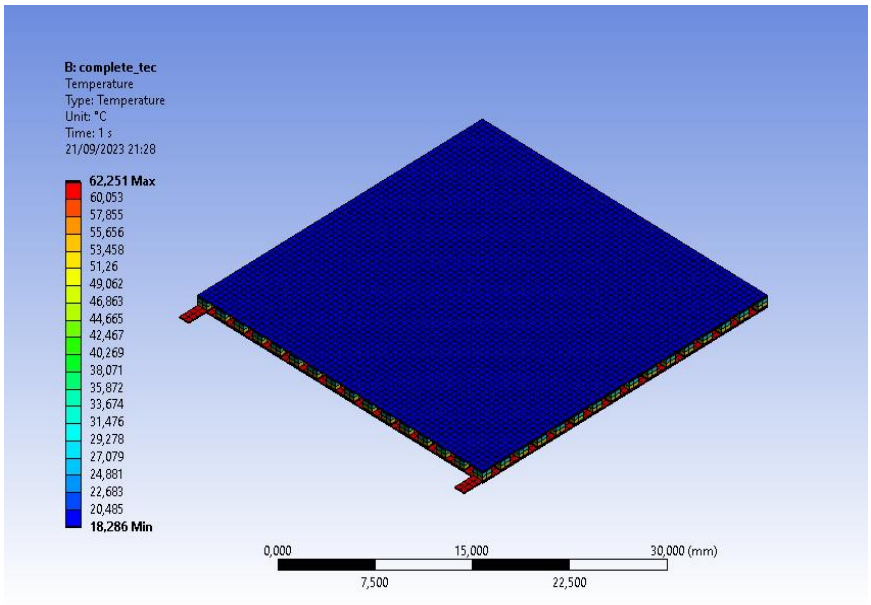

Figure 7. Numerical FEM simulation in steady state of a full TEC.

As shown in Figure 7, the numerical simulation at steady state worked alongside as it occurs at the first bench experiment, reaching almost the same values, being now both validated, seeing that after boundary conditions had been applied at all the elements from Table 4, it was attainable to reach a 62ºC temperature of on the hot side, and as a result an 18ºC on the cold side. However, the temperature achieved at the cold side of each simulation was not the one we were looking for (which is 4ºC to 9 °C). Nevertheless, to reach our goal, were introduced to the second bench experimental, two fans, coupled at the heat sink sides, adding forced convection, regard to reduce the temperature at cold side and increased heat dissipation at hot side.

The results from the second bench experiment are shown in Figure 8, which indicates that our prototype will be operating. In Figure 8, the second experimental bench was carried out under the conditions of forced convection (with two fans attached to the heat sink), and the room air-conditioning was turned off (reaching 24ºC room temperature). As we can see, all temperature data start almost at the same point, and when the current is applied, it took approximately a few seconds to reach -5 °C and -7 °C and continued until the end of the experiment; meanwhile, on the hot side, the temperature rose and stabilizes at approximately 27ºC, which is different from the results of the first bench experiment Figure 6. This means that the introduction of forced convection helped the system reach what we were expecting, and the Joule effect had less impact on the system than before.

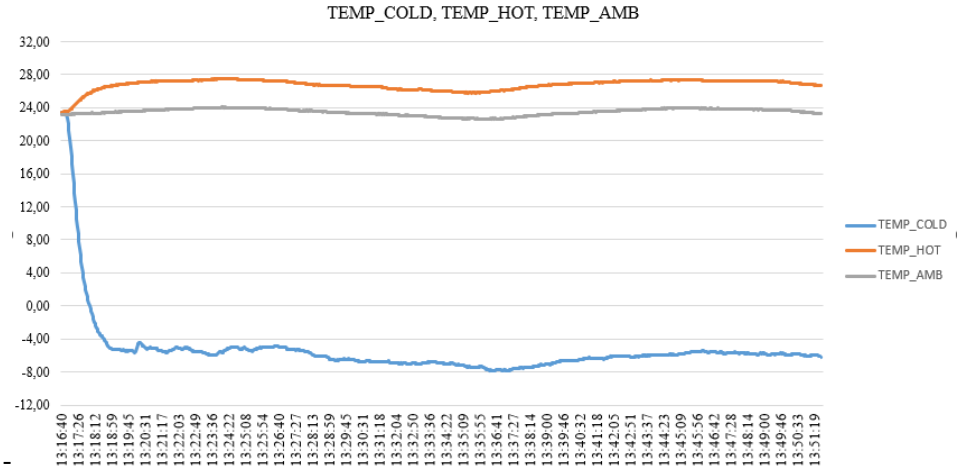

Figure 8. Temperature data from the second bench experiment.

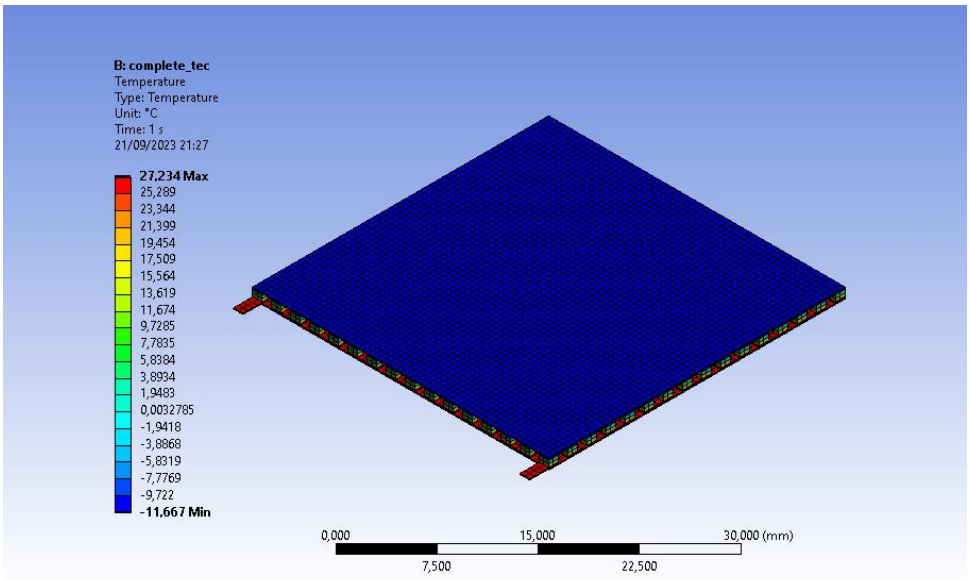

Figure 9. Second numerical simulation.

Figure 9 shows the results of the second numerical simulation, taking as input the BCs from Table 5. The output temperatures on the cold side reached -11.66ºC, but when compared with the result on the experimental side in Figure 8, there is a temperature difference of 3ºC, which may have been caused by measurement errors associated with the temperature sensors, the location where the sensors are measuring or the amount of thermal load in the laboratory (people, doors being opened/closed, etc.). It is conclusive that there are errors associated with the bench experiment and perhaps the numerical simulation, but to know which of the two is causing this, we will carry out a statistical analysis and publish it in future work.

4. CONCLUSION

Based on the presented and discussed results, it is feasible to attain temperatures below 10ºC. This possibility arises from the decrease in temperature on the hot side when forced convection is added to the heat sink rather than using natural convection. However, it is not just this; with this configuration, the Joule Effect also decreases, having less impact on the cold side, since we know heat transfer occurs from the highest to the coldest temperature. Nevertheless, it is plausible to highlight the successful validation of numerical simulations and bench experiments because what was proposed was achieved.

Although using only forced convection attached to the heat sink shows that we have the potential to seek temperatures below 10 °C, we are looking to implement a more efficient, small device that does the same job, or even better, because the main goal of this prototype is to be portable, and by using a large device will be controversial.

Problems were encountered in the second experimental and numerical simulations, referring to the temperature difference of 3ºC, which may be associated with measurement errors in the temperature sensors, the places where they are measuring, the heat load of the people in the laboratory, etc.; and the solution will be a statistical analysis of the errors in the system to confirm which one is causing this problem. Despite the associated errors, we can confirm that we have achieved the desired temperature value.

A solution to the problem of the size of the heat sink could even be an assembly of water coolers, with different kinds of fluids (e.g., graphene nanotubes, water, radiator fluids, etc.), and with all these new ideas we are willing to implement, we will first carry out a numerical simulation to see how they will work and confirm the simulation with an experimental test. Finally, these data will be crossed to determine which one is better from all perspectives, from economics to production and portability.

In the end, the results obtained provide a starting point for building a refrigerated TEC prototype for transporting organs, vaccines, and medicines. It is more efficient and safer, allowing customization of temperature control for the transported material when compared to the traditional method currently applied.

5. ACKNOWLEDGEMENTS

All the authors thanks IFPE for his support through this project's development. The fourth author thanks the CNPq for the Productivity Grant 3303417/2022-6.

6. REFERENCES

Silvester P. P. and Ferrari, R. L., 1996 .Finite Elements for Electrical Engineers, 3rd Edition, University Press (Cambridge).

Canuto, César Borelli; Biasotto, Tiago Ramos., 2018. Modelagem e Controle de um Sistema Termoelétrico Aplicado à Conservação de Medicamentos Termolábeis. UFPR.

Souza, Thierry Kaue A.S., 2019. Cartilha: O ABC dos Transplantes. Unicamp.

Nohay, Julian Albert D.; De Belen, John Karl H.; Claros, John Vernon B.; Lupo, Ron Benjo P.; Barrato, Amiel Benedict; Dela Cruz, Jennifer C.; Amado, Timothy M.; Manuel Mark Christian E., 2020. Design and Fabrication of a Portable Solar Power Thermoelectric Refrigerator for Insulin Storage. ICSGRC.

Ivanov, Kaloyan; Belovski, Ivaylo; Aleksandrov, Anatoliy., 2021. Desing, Building and Study of a Small-size Portable Thermoelectric Refrigerator for Vaccines. ELMA.

Daimon, Shunsuke; Iguchi, Ryo; Hioki, Tomosato; Saitoh, Eiji; Uchida, Ken-ichi., 2016. Thermal Imaging of Spin Peltier Effect. Nature Communications.

Antonova, Elena E.; Looman, David C., 2005. Finite Elements for Thermoelectrics Device Analysis in Ansys. International Conference on Thermoelectrics.

Bhyiyan, Sadequr Rahman; El-Shahat, Adel., 2019. Thermoelectric Generator Analysis Through Ansys and Matlab/Simulink. SoutheastCon.

Seifert, W.; Ueltzen, M.; Muller, E., 2002. One-dimensional Modelling of Thermoelectric Cooling. Physica Status Solid Applications and Materials Science, Vol 194, p. 277-290.

Jaegle, Martin; Bartel, Markus; Ebling, Dirk; Bottner, Alexandre Jacquot Harald., 2014. Multiphysics simulation of thermoelectric systems. Fraunhofer-Institute for Physical Measurement Techniques.

Chen, Lidong; Liu, Ruiheng; Shi, Xun., 2021. Thermoelectric Materials and Devices. Elsevier, 1st Edition.

Incropera, Frank P.; DeWitt, David P.; Bergman, Theodore L.; Lavine, Adrienne S., 2006. Introduction to Heat Transfer. Wiley, 5th Edition.

MacKnight, Patrick T., 2010. Finite Element Analysis of Thermoelectric Systems with Applications in Self Assembly and Haptics. USF Tampa Graduate Theses and Dissertations.

Barrubeeah, Mohammed; Rady, Mohamed; Attar, Alaa; Albatati, Faisal; Abuhabaya, Abdullah., 2021. Design, modeling and parametric optimization of thermoelectric cooling systems for high power density electronic devices. International Journal of Low-Carbon Technology, p. 1060-1076.

7. RESPONSIBILITY NOTICE

The author(s) is (are) the only responsible for the printed material included in this paper.